Available online at www.sciencedirect.com

ScienceDirect

IFAC Papers Online CONFERENCE PAPER ARCHIVE

IFAC PapersOnLine 51-2 (2018) 174–179

Numerical Identification of Motor Units using an Optimal Control Approach

Sproll, Tobias * **Schiela, Anton** ** **Lowery, Madeleine** ***

* *University of Bayreuth (e-mail: tobias.sproll @ uni-bayreuth.de)*
** *University of Bayreuth(e-mail: anton.schiela @ uni-bayreuth.de)*
*** *University College Dublin (e-mail: madeleine.lowery @ ucd.ie)*

Abstract: A numerical approach to locate motor units in human muscles by high density surface EMG measurements is presented. For this purpose a mathematical model has been derived which can be evaluated by finite element computations. On that basis an optimal control problem is specified that can be solved by a function space oriented optimization method. Numerical results are reported for a test problem.

Keywords: Optimal control, Finite elements, Electromyography, Medical applications, Biomedical modeling

1. INTRODUCTION

High density surface Electromyography (sEMG), is a non-invasive method of measuring the activity of muscles whereby an array of electrodes is placed above the skin and a spatially and temporally resolved measurement of the electric potential on the skin is obtained. Recent advances in high-density sEMG measurement have opened the possibility of extracting information about single motor units (groups of muscle fibers controlled by the same motor neuron) from the sEMG signal.

While significant advancements have been made in identifying the activity of individual motor units from the surface EMG signal through EMG decomposition methods (cf. e.g. Kleine et al. (2007)), a reliable and accurate method to determine from the sEMG signal where the motor units are located and where the trajectory of the muscle fibers run is not yet available. Previous works consider spatial data only [van den Doel et al. (2008, 2011); Liu et al. (2015)] or use simple parametric models within a least squares approach [Mesin (2015)].

In this work we describe an approach to automate the identification of motor units using techniques from numerical simulation and non-linear optimization.

Acknowledgment The authors would like to thank Prof. Dr. Dr. Bernd Lapatki (Department of Orthodontics, University of Ulm, Germany) for bringing them into contact and drawing their interest on the topic and Dr. Hans van Dyck (Department of Orthodontics, University of Ulm, Germany) for helpful discussions on the subject.

2. CONDUCTION OF ACTION POTENTIALS

The basis of our approach is a mathematical model for the physiology and for the physical situation.

2.1 Propagation of electric fields in the human body

Consider some part of the body, e.g. a limb or a part of the head, represented by a Lipschitz domain $\Omega \subset \mathbb{R}^3$ with sufficient smooth boundary Γ. We denote the spatial variable by $x \in \Omega$ and the temporal variable by $t \in [0, T]$. We are interested in the electric potential $\Phi(x, t)$ in Ω caused by a given distribution of electric charge $\rho(x, t)$.

The human body consists of various types of tissue with different physical properties. We assume that the different tissues behave like a volume conductor [Stegeman et al. (2000) and Lowery (2016)]. This means Ohm's law is applicable and thus $\Phi(x, t)$ can spread out in the domain and can therefore be measured at the surface. Like the majority of previous sEMG simulation studies we assume that at the frequencies of interest the tissue is purely resistive and its conductivity $\sigma(x)$ is independent of Φ [Stegeman et al. (2000), Lowery (2016) and Gootzen et al. (1991)]. For skin and subcutaneous fat tissue we assume that σ is isotropic [Stegeman et al. (2000),Lowery (2016), Andreassen and Rosenfalck (1981) and Gootzen et al. (1991)]. For muscle tissue however one assumes that the conductivity is anisotropic, i.e. that the conductivity is higher along the fiber axis.

On Γ we impose different kinds of boundary conditions. In the part of the boundary Γ_0 where skin is adjacent to air we note that in general the electrical potential in air is zero. Further we assume that there are no sources outside of the domain and thus we get the following Robin-boundary condition

$$\partial_\nu \Phi(s, t) = -\mu \Phi(s, t) \quad \text{at } \Gamma_0$$

with skin conductivity μ. In addition, since we only model a part of the body, there are artificial boundaries $\Gamma \setminus \Gamma_0$ that result from removing the rest of the body. We assume that the potential is zero for all points which are far away from the inner source and thus we get homogeneous Neumann boundary conditions.

As usual we can write now the electric potential equation and the boundary conditions in the weak form with a solution $\Phi(\cdot, t) \in H^1(\Omega)$

10.1016/j.ifacol.2018.03.030

$$\int_\Omega \rho(x,t)v(x)\mathrm{d}x = \int_\Omega \sigma(x)\nabla\Phi(x,t)\nabla v(x)\mathrm{d}x + \int_{\Gamma_0} \mu\Phi(s,t)v(s)\mathrm{d}s \quad \forall v \in H^1(\Omega) \tag{1}$$

We remark that the left hand side is well defined, for $\rho(\cdot,t) \in L_2(\Omega)$. However, this equation can still be formulated rigorously for concentrated charges, i.e., if $\rho(\cdot,t)$ is a measure on Ω, if v is chosen in $W^{1,p}(\Omega)$ with $p > 3$. Then it is known (cf. e.g. Haller-Dintelmann et al. (2009); Alibert and Raymond (1997)) that $\Phi(\cdot,t) \in W^{1,p'}(\Omega)$ for $1/p + 1/p' = 1$.

In our model the charge distribution $\rho(\cdot,t)$ in (1) is caused by ionic activity, the so called action potential that propagates along the muscle fiber of a motor unit and activates the contraction of the muscle. Its definition will be explained in the following two subsections.

2.2 Motor units

A motor unit is a bundle of muscle fibers which are innervated by the same motor neuron. The motor unit is the smallest controllable unit of a muscle. If now a muscle fiber is activated, two action potentials propagate in opposite directions from the neuro-muscular junction to the ends of the muscle fiber. The velocity v with which the action potential propagates is almost constant. In general the neuro-muscular junction lies approximately in the middle of the fiber. In Figure 1 one can see a schematic view of such a motor unit. As all of the fibers within

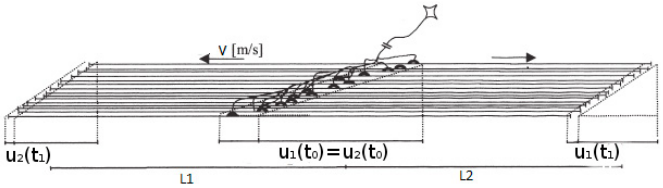

Fig. 1. Sketch of a motor unit [Stegeman et al. (2000)]

a motor unit are activated simultaneously, we can treat a bundle of muscle fibers in a motor unit as a single fiber. For such a fiber we assume that the radius (a few μm) is much smaller than its length (several cm) [Andreassen and Rosenfalck (1981) and Gootzen et al. (1991)] and thus we can represent the trajectory of the moving action potential along the fibers by a pair of regular curves

$$u_1, u_2 : [t_0, t_1] \mapsto \Omega_m$$
$$u_1, u_2 \in V := H^1([t_0, t_1])^3.$$

The point $u_1(t_0) = u_2(t_0)$ represents the neuro-muscular junction and $u_1(t_1)$ and $u_2(t_1)$ represent the fiber ends. With $\dot{u}_k(\tau) := \frac{d}{d\tau}u_k(\tau)$ we denote the tangent vector of the curves.

2.3 Propagating action potentials

Before we define the action potential and thus also the source density we make some assumptions. First we assume that only one motor unit is active and thus the support of the source density ρ is included in the curves, i.e.

$$\rho(x,t) = 0 \quad \forall t \in [0,T]\,,\ x \notin u_k([t_0,t_1]),\ k = 1,2. \tag{2}$$

Therefore ρ is a measure with support on u_k. Furthermore we assume that the source density fulfills the condition

$$\int_\Omega \rho(x,\cdot)dz = 0 \tag{3}$$

which expresses the conservation of charge in the human body.

We now consider that the source density is a spatially distributed signal, the so called action potential, which propagates along a trajectory of a motor unit. Similar to Rosenfalck (1969) we define the action potential in terms of an artificial real variable z as follows:

$$i_m(z - z_0(t)) := \begin{cases} \sigma_{in}\pi r^2 \dfrac{d^2V_m(z - z_0(t))}{dz} & \text{if } z \le z_0 \\ 0 & \text{if } z > z_0 \end{cases} \tag{4}$$

where $\frac{d^2V_m(z)}{dz} = -96\exp(z)(6z + 6z^2 + z^3)$ is the second spatial derivative of the transmebran potential, σ_{in} is the intracellular conductivity and r is the radius of the motor unit. Here we changed the orientation of the action potential, by replacing z through $-z$ in V_m, and added the origin of the signal $z_0(t) := v(t - t_0)$. With this modification we generate a signal which propagates in time from left to right along the artificial axis as the time t increases. This moving action potential can be seen in Figure 2 for three different times.

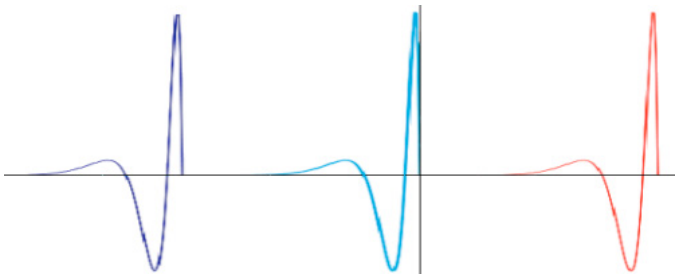

Fig. 2. Moving action potential at different times t

For fixed t we can now uniquely identify each point on the trajectory u_k with a point $\tilde{z} \in [0, L_k]$ by the arc length of the corresponding curve segment. Here L_k is the the length of the trajectory u_k. Thus we can define the diffeomorphism

$$z(u_k(\tau)) := \int_{t_0}^{\tau} |\dot{u}_k(\xi)|d\xi. \tag{5}$$

If we combine now (2), (4) and (5) we get for the source density

$$\rho(x,t) = \begin{cases} i_m(z_k(\tau) - z_0(t)) & \text{if } x = u_k(\tau) \\ 0 & \text{else} \end{cases}. \tag{6}$$

One can now easily proof that the source density fulfills the condition (3).

2.4 End-effects

By the simulation of sEMG it is well known, that if the fiber length is finite, so called end-effects can appear [Gootzen et al. (1991)] and thus we have to correct our model of the source density. Before we can correct the model of the source density we have to explain when and why those end- effects appear. To this end we simulated an sEMG measurement with our current model. In Figure 3 one can see the result of a simulation with the current model (red graph). Here we simulated a straight fiber and the electrode was positioned in the middle between the

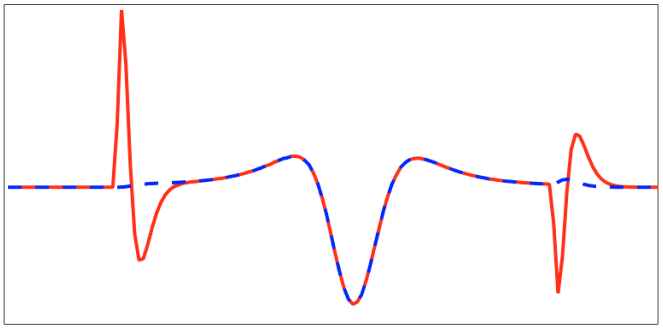

Fig. 3. Comparing the corrected simulation (dashed blue) with the uncorrected simulation (red)

neuro-muscular junction and one end of the fiber. Comparing the simulation with real measurements one can easily see that there appear some unphysical peaks at the left and right end of the measurement. We have noted before in the modeling that the integral over the full support of the action potential is zero (compare (3)), but since the signal is represented through a moving stationary source it can happen that not the full support of the signal lays on the curve which leads to an imbalance of charges in the tissue. There are two possible situations when such an imbalance can appear, namely when the signal arrives at the neuro-muscular junction ($t \in I_0$) and when the signal vanishes at the fiber end($t \in I_1$). One possibility for correcting this imbalance is given in [Gootzen et al. (1991)] by adding a term g that represents stationary sources at the fiber-ends. These term has then to be chosen such that

$$\int_{u_k} \rho(x,t)dx + g(u_k(t_0),t) + g(u_k(t_1),t)dx \stackrel{!}{=} 0.$$

Furthermore we assume that

$$g(u_k(t_0),t) = 0 \quad \text{if } t \in I_1$$
$$g(u_k(t_1),t) = 0 \quad \text{if } t \in I_0$$

holds, which means that only one correction term is not equal to zero at the same time. This assumption is only sufficient if the lengths of the curve is longer than the support of the action potential. In our model problems we will assume that this is always true. With this assumption we get for the correction terms

$$g(u_k(t_0),t) = \begin{cases} -\int_{t_0}^{t_1} |\dot{u}_k(\tau)| i_m(z(u_k(\tau)) - z_0(t))d\tau & \text{if } t \in I_0 \\ 0 & \text{else} \end{cases}$$

$$g(u_k(t_1),t) = \begin{cases} -\int_{t_0}^{t_1} |\dot{u}_k(\tau)| i_m(z(u_k(\tau)) - z_0(t))d\tau & \text{if } t \in I_1 \\ 0 & \text{else} \end{cases}$$

If we now add these correction terms to the source density and simulate again the measurement, one can see that the end effects has almost vanished (see green graph in Figure 3).

3. ADJOINT APPROACH

In the previous section we have described the mapping $(u_1, u_2) \to \Phi$, where Φ is defined on the space-time cylinder $\Omega \times [0,T]$. Although our problem is merely quasi-static, the evaluation of this mapping for reasonably high temporal and spatial resolution is computationally expensive, in particular if this evaluation has to take place multiple times within an optimization algorithm. However, by sEMG measurements, only part of the information that is present in Φ is actually used. Measurements are taken only at finitely many electrodes $D_i \subset \Gamma_0$ on the skin, given by

$$\tilde{y}_i(t) = \int_{D_i} \Phi(s,t)ds \quad \text{for } t \in [0,T].$$

For fixed t each measurement is thus a linear functional $l_i : H^1(\Omega) \to \mathbb{R}$ with argument $\Phi(\cdot, t)$.

To reduce the numerical effort of evaluating $\tilde{y}_i$ we now introduce an alternative way to compute the measurements. The scalar quantity

$$\tilde{y}_i(t) = l_i(\Phi(\cdot,t)) \quad \text{for } t \in [0,T]$$

can be evaluated efficiently by the following formula

$$\tilde{y}(t) = \int_\Omega w(x)\rho(x,t)dx \tag{7}$$

where w is the solution of the adjoint problem

$$\int_\Omega \sigma(x)\nabla w(x)\nabla v(x)\mathrm{d}x + \int_{\Gamma_0} \mu w(s)v(s) - \mathbf{1}_{D_i} v(s)\mathrm{d}s = 0. \tag{8}$$

This formula follows from the following simple abstract computation: Let $\Phi \in V$ satisfy:

$$a(\Phi, v) = r(v) \quad \forall v \in W,$$

where $a : V \times W \to \mathbb{R}$ is bilinear and $r \in W^*$ is linear. Let further w satisfy:

$$a(\phi, w) = l(\phi) \quad \forall \phi \in V,$$

then

$$l(\Phi) = a(\Phi, w) = r(w).$$

4. OPTIMAL CONTROL PROBLEM

Now we assume that we have a measurement array with J electrodes. For each of these electrodes we can compute a weight function w_j by solving the adjoint problem (8). If we now define the vector $w = (w_0, ..., w_J)$ we can, by using the model (7), compute the vector valued potential with the vector valued integral

$$y(t,u) = \sum_{k=1}^{2} \Bigg[\int_{t_0}^{t_1} w(u_k(\tau))|\dot{u}_k(\tau)| i_m(z_k(\Theta_k(\tau),t))d\tau + w(u_k(0))g(u_k(0),t) + w(u_k(1))g(u_k(1),t) \Bigg] \tag{9}$$

such that the potential at the electrode j is the j-th component of y. Furthermore with $y_m(t)$ some measured potential at the electrodes is given. For our optimal control problem we then want to minimize the L^2-norm of the distance between measurement and simulation. Additionally we add a penalty term which shall ensure that the speed of the curve is nearly constant and equal in magnitude to a given reference velocity v_r. We get then the following optimization problem

$$\min J(u) = \|y(u,t) - y_m(t)\|^2_{L_2([0,T])} + \frac{\alpha}{2} c(u) \tag{10}$$

with

$$c(u) = \int_{t_0}^{t_1} (|\dot{u}(\tau)| - v_r)^2 \mathrm{d}\tau$$

5. NUMERICAL IMPLEMENTATION

In this section we take a closer look on how to solve the above stated optimization problem. First we specify the geometric setting. As domain Ω we choose a cuboid with size $10cm \times 10cm \times 1cm$. This cuboid shall represent an idealized piece of some limb. We divide this cuboid into two horizontal layers where the lower layer has a thickness of $8mm$ and represents the muscle tissue. The second layer is $2mm$ thick and represents a fat layer under the skin. Furthermore we define the upper boundary as Γ_0 where the domain is bounded by skin. At the other boundaries we assume that the domain would continue. One can see a schematic view of this cuboid in Figure 4. On the

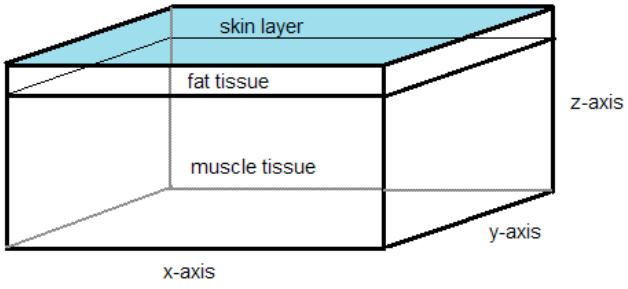

Fig. 4. Schematic view of the domain

time interval $[0s, 0.015s]$ we generate artificial measurements by forward simulation. The action potential is active in the sub interval $[t_0, t_1] = [0.0025s, 0.0125s]$, which is the domain of the trajectories. Finite element discretization of the spaces $H^1(\Omega)$ and $H^1([t_0, t_1])^3$ is performed as follows. We choose a triangulation $\mathfrak{T}$ of Ω and a triangulation $\mathfrak{U}$ of the interval $[t_0, t_1]$. The domain Ω is thereby divided into tetrahedrons, whereas the I is simply divided into n intervals. Using this triangulation we can then define the space of linear ansatz functions for $H^1([t_0, t_1])^3$ and the space of quadratic ansatz functions for $H^1(\Omega)$ by

$$V_n := \{v : [t_0, t_1] \mapsto \mathbb{R}^3 \mid v|_K \in P_1(K) \, \forall K \in \mathfrak{U}\} \subset V$$
$$W_n := \{w : \Omega \mapsto \mathbb{R} \mid w|_K \in P_2(K) \, \forall K \in \mathfrak{T}\} \subset H^1(\Omega)$$

The corresponding finite element method is implemented with the help of the finite element Toolbox Kaskade7 [Götschel et al. (2012)].

5.1 Solving the adjoint problem

For the optimization it is essential to compute the weight functions w by solving the adjoint problem and to be able to evaluate them at each point in the domain Ω. Since we have to compute, store and evaluate the weight functions efficiently, we decided to use a hierarchically and adaptively built triangulation of Ω. Therefore we first generate a coarse grid and refine it globally to a certain mesh size. After that we refine then the area where the electrodes are placed and the the area where the optimal solution is expected to be. One possible triangulation can be seen in Figure 5. We then use a Galerkin-Method to solve the adjoint problem (7). As usual this leads to the discrete replacement problem

$$\text{find } w_n \in W_n \text{ s.t.}$$
$$a(w_n, \eta) = r(\eta) \quad \forall \eta \in W_n \qquad (11)$$

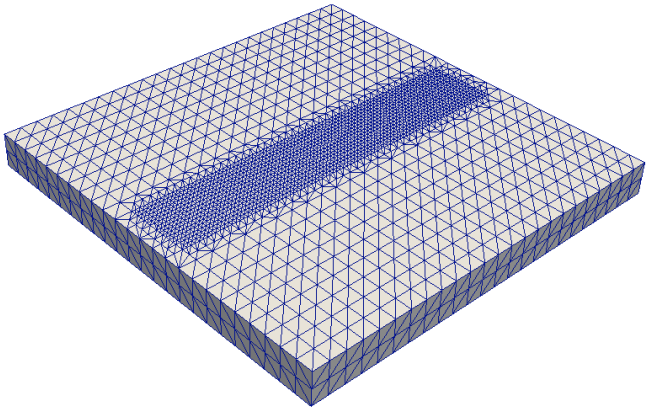

Fig. 5. Mesh with about 750000 tetrahedrons. In the critical region the mesh has been refined, a-priori.

With the usual techniques one can show that the bilinear form $a(\cdot, \cdot)$ is V-elliptic and since r is a bounded linear functional one knows from the Lemma of Lax-Milgram that the problem (11) has a unique solution.

After finite element discretization we end up with a large sparse linear system of equations that we solved with the preconditioned conjugate gradient method. Here we use a BPX-preconditioner [Bramble et al. (1990)], which takes advantage of our hierarchic grid.

5.2 Evaluation of weight functions

As we have seen in (9) and (10), the objective function of our optimal control problem depends on line integrals that involve the weight functions w_j, evaluated along given trajectories. For optimization purposes we also have to evaluate spatial derivatives of w, i.e., w_x and w_{xx} to compute the derivative and the hessian of the objective, since a small perturbation of u_k leads to a perturbation of the points, where w is evaluated.

Since w is only available as a finite element function we cannot expect w_x to be continuous. Even more, w_{xx} is only defined in the interior of the tetrahedrons, and may not properly reflect the global curvature of the solution. For example $w_{xx} = 0$ for linear finite elements. Nevertheless, there are theoretical results available (cf. Ovall (2007)) that indicate that second derivatives of finite element functions of order higher than one asymptotically approximate second derivatives of regular solutions of elliptic PDEs. In our numerical experiments the convergence behavior of our optimization algorithm depends on the resolution of the finite element discretization (see Figure 8 below). We observe fast linear convergence, the finer the grid, the faster the rate. The deeper understanding of this interesting phenomenon is subject to current investigations.

The evaluation of the line integrals is performed by numerical quadrature along u_k. The necessary evaluation of the finite element function w at a quadrature point x requires a search for the tetrahedrons where x is located. To do this efficiently we exploit that the quadrature points are ordered along the trajectory and thus use a neighborhood search. If this fails, we fall back to a hierarchic search over the whole grid.

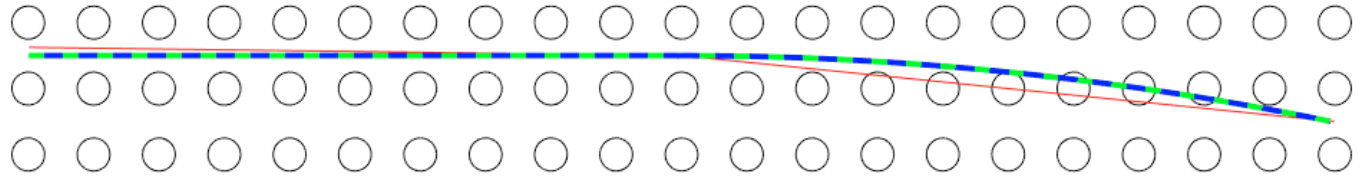

Fig. 6. Position of the electrodes and comparison of the reference trajectory (green), the start trajectory (red) and the computed solution (dashed blue) in the xy-plane.

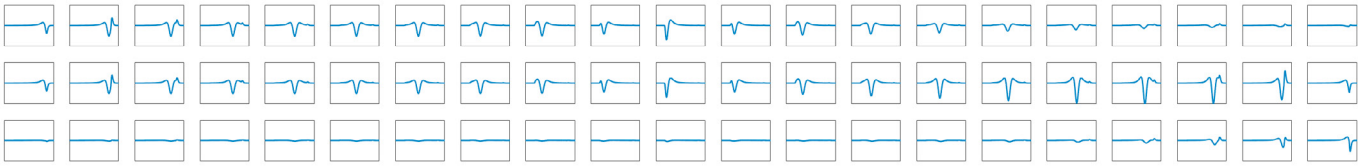

Fig. 7. Simulated measurement data at the array of electrodes. In each square the temporal signal of the corresponding electrode is displayed.

5.3 Numerical solution of the optimization problem

To solve the minimization problem we use a simple SQP line search method. This means in each step we compute a direction of descent δu and a sufficient step size β. For the computation of a step we establish a quadratic model of the functional by

$$J(u+\delta u) \approx m_u(\delta u) := J(u) + J'(u)\delta u + \frac{1}{2} q_u(\delta u, \delta u).$$

The bilinear form

$$q_u(\delta u, \delta u) = J''(u)(\delta u, \delta u) + \gamma \|\delta u\|^2_{V\times V}$$

employs second order information of J. The term $\gamma\|\delta u\|^2_{V\times V}$ is added to overcome possible indefiniteness of $J''(u)$. So γ is chosen adaptively to make q_u positive definite, if $J''(u)$ isn't. We thus have a modified Hessian-method which differs from classical modified Hessian methods by the choice of regularization term.

To get the direction of descent from this model one has then to minimize $m_u(\delta u)$ over δu which is equivalent to solving the variational problem

$$\text{find } \delta u \in V_n \times V_n \text{ s.t.}$$
$$q(\delta u, \eta) = J'(u)\eta \;\forall \eta \in V_n \times V_n \qquad (12)$$

Since u is defined on a one dimensional domain this problem is of moderate size after discretization and can thus be solved by a Cholesky factorization.

For the so computed direction it remains to compute a sufficient step-size. We do this by using a simple backtracking algorithm with Armijo acceptance criterion as one can find it e.g. in [Nocedal and Wright (2006)]. Finally we get the following simple optimization algorithm 1:

Algorithm 1. (line search).

choose u_0
while $J'(u_k)\delta u_k > \epsilon$ **do**
  solve $q(\delta u_k, \eta) = -J'(u_k)\eta$
  compute step length β
  $u_{k+1} = u_k + \beta\delta u_k$
end while

6. NUMERICAL EXAMPLE

To test the above described algorithm we first simulate a measurement for a reference trajectory $\tilde{u}$. Therefore we choose a measurement array of 63 electrodes, which are placed in three rows of 21 electrodes above the reference trajectory. The electrodes have the shape of circles with diameters of $2\,mm$ and the distance between the centers of two neighboring electrodes is $4\,mm$. In Figure 6 we illustrate the setting, by plotting the the position of the electrodes at the skin (black circles) and the reference trajectory (green). We divide then our time interval $[0.0025s, 0.0175s]$ into 150 time steps and compute for each electrode the potential $y_i(t_k)$ at each time step t_k. From this measured potential one can then make an initial guess for the starting trajectory by placing it in the regions were the highest potential is measured. This is also a good option in practical applications. In Figure 6 one can also see our choice for the starting trajectory (red).

From this measurement we then identify the reference trajectory with our optimization algorithm. For this example we assume that we know the interval $[t_0, t_1]$, the velocity v of the signal, which is $4\frac{m}{s}$, and the position of the neuro-muscular junction $u_1(t_0) = u_2(t_0)$. The position of the fiber ends $u_1(t_1)$ and $u_2(t_2)$ and the depth of the trajectory are unknown and shall be identified during the optimization.

We stop the algorithm when the energy norm of the gradient is sufficiently small, i.e. $J'(u)\delta u \leq 10^{-9}$. In Figure 6 one can see the computed solution (dashed blue) compared to the reference trajectory (green). One can see that the reference trajectory is identified very well by the solution of our optimization problem, the two graphs coincide.

To assess the influence of the discretization of the weight functions we performed the optimization with two different grids for the computation of w. In the first run we used approximately 750000 tetrahedrons. In a second run we reduced the mesh of 142000 tetrahedrons. It can be observed that both solutions are quite similar in accuracy, but the rate of convergence differs significantly. For the coarse solution, about 14 iterations are needed, while the fine solution requires only 8 iterations. We attribute this behavior to the fact that more accurate second order information is available for the fine solution. To illustrate

this we compare in Figure 8 the energy norm of the gradient for the different mesh sizes.

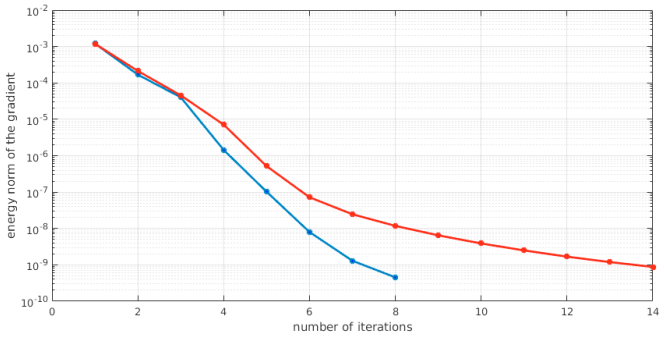

Fig. 8. Comparison of the energy norm of the gradient for 750000 tetrahedrons (blue) and 142000 tetrahedrons (red)

7. CONCLUSION

We have constructed a numerical algorithm that can take into account the full spatio-temporal information, gained by high-density sEMG measurements in order to locate motor units in human muscles. It is based on an accurate finite element model of the physiological situation. An adjoint approach makes the problem tractable numerically. For a test problem our optimization method converges in a few iterations and yields accurate results.

In future research our method has to be applied to real measurement data to assess the accuracy of our forward model and the influence of modeling errors and noisy data on the identified solution. From a numerical point of view, adaptive solution techniques for the computation of the weight functions as well as for the trajectories will be explored. Finally, a deeper understanding of the accuracy of the spatial derivatives of w is desirable, giving rise to further theoretical investigations.

REFERENCES

Alibert, J.J. and Raymond, J.J. (1997). Boundary control of semilinear elliptic equations with discontinuous leading coefficients and unbounded controls. *Numerical Functional Analysis and Optimization*, 18(3-4), 235–250.

Andreassen, S. and Rosenfalck, A. (1981). Relationship of intracellular and extracellular action potentials of sceletal muscle fibers. *CRC CriticalReviews in Bioengineering*, 267–306.

Bramble, J.H., Pasciak, J.E., and Xu, J. (1990). Parallel multilevel preconditioners. *Math. Comp.*, 55(191), 1–22.

Gootzen, T., Stegeman, D., and Van Oostrom, A. (1991). Finite limb dimensions and finite muscle length in a model for the generation of electromyographic signals. *Electroencephalography and clinical Neurophysiology*, 152–162.

Götschel, S., Weiser, M., and Schiela, A. (2012). Solving optimal control problems with the Kaskade7 finite element toolbox. In A. Dedner, B. Flemisch, and R. Klöfkorn (eds.), *Advances in DUNE*, 101 – 112. Springer.

Haller-Dintelmann, R., Meyer, C., Rehberg, J., and Schiela, A. (2009). Hölder continuity and optimal control for nonsmooth elliptic problems. *Applied Mathematics and Optimization*, 60(3), 397–428.

Kleine, B.U., van Dijk, J.P., Lapatki, B.G., Zwarts, M.J., and Stegeman, D.F. (2007). Using two-dimensional spatial information in decomposition of surface EMG signals. *Journal of Electromyography and Kinesiology*, 17(5), 535 – 548.

Liu, Y., Ning, Y., Li, S., Zhou, P., Rymer, W.Z., and Zhang, Y. (2015). Three-dimensional innervation zone imaging from multi-channel surface emg recordings. *International Journal of Neural Systems*, 25(06), 1550024.

Lowery, M. (2016). *Surface Electromyography: Physiology, Engineering and Applications*. US: Wiley-IEEE Pressr. Chapter, EMG Modeling and Simulation.

Mesin, L. (2015). Real time identification of active regions in muscles from high density surface electromyogram. *Computers in Biology and Medicine*, 56, 37–50.

Nocedal, J. and Wright, S. (2006). *Numerical Optimization*. Springer.

Ovall, J.S. (2007). Function, gradient, and Hessian recovery using quadratic edge-bump functions. *SIAM J. Numer. Anal.*, 45(3), 1064–1080.

Rosenfalck, P. (1969). *Intra- and extracellular potential fields of active nerve and muscle fibres*. Acta physiologica Scandinavica / Supplementum.

Stegeman, D.F., Blok, H.F., Hermens, H., and Roeleveld, K. (2000). Surface EMG models: properties and applications. *Journal of Electromyography and Kinesiology*, 313–326.

van den Doel, K., Ascher, U.M., and Pai, D.K. (2008). Computed myography: three-dimensional reconstruction of motor functions from surface emg data. *Inverse Problems*, 24(6), 065010.

van den Doel, K., Ascher, U.M., and Pai, D.K. (2011). Source localization in electromyography using the inverse potential problem. *Inverse Problems*, 27(2), 025008.